Optical Materials: X 20 (2023) 100257

Contents lists available at ScienceDirect

Optical Materials: X

journal homepage: www.journals.elsevier.com/optical-materials-x

Luminescent properties of the $Sr_{8-x}Ba_xMgY(PO_4)_7:Eu^{2+}$ solid solution

Nakyung Lee [a,b], Małgorzata Sójka [a,b], Jakoah Brgoch [a,b,*]

[a] Department of Chemistry, University of Houston, Houston, TX, 77204, USA
[b] Texas Center for Superconductivity, University of Houston, Houston, TX, 77204, USA

ARTICLE INFO

Keywords:
Solid state lighting
Inorganic phosphor
Photoluminescence
Whitlockite

ABSTRACT

Photoluminescence generated by substituting rare-earth ions on multiple crystallographically independent cation sites within a crystalline host material is one of the most common approaches for creating a full-spectrum phosphor-converted white light-emitting diode (pc-wLED). In this work, a series of complex orthophosphates with the composition $(Sr_{8-x}Ba_x)_{0.99}Eu_{0.08}MgY(PO_4)_7$ (x = 0, 1, 2, 3) were synthesized via high-temperature solid-state synthesis. These materials possess five potential substitution sites achieving broadband (5905 cm^{-1}) yellow photoluminescence through multi-site substitution showing a violet-excited photoluminescent quantum yield of nearly 50%. Developing such an efficient broad emission spectrum is crucial for enhancing the color rendering ability of pc-wLEDs. Varying the Sr^{2+} to Ba^{2+} shifts the emission color from green-yellow to yellow under violet excitation (λ_{ex} = 400 nm) while influencing the full-width-at-half-maximum (*fwhm*). Temperature-dependent photoluminescence measurements indicate that phosphor has good thermal stability with T_{50}, the temperature at which the emission intensity is half of the low-temperature intensity, at 420 K and stable chromaticity coordinates, further supporting that the $(Sr_{8-x}Ba_x)_{0.99}Eu_{0.08}MgY(PO_4)_7$ series are promising candidates for LED white lighting. Constructing a prototype pc-wLEDs device using $(Sr_7Ba)_{0.99}Eu_{0.08}MgY(PO_4)_7$, the highest quantum yield phosphor, produced a functional daylight bulb with a color rendering index (CRI) of 90.

1. Introduction

Phosphor-converted light emitting diodes (pc-LEDs) have become the leading choice for home and commercial lighting over incandescent and fluorescent lighting owing to their superior energy efficiency, prolonged operational lifetimes, and environmentally safe components [1,2]. In these devices, phosphors, comprising an inorganic host structure and an activator ion, play a crucial role in creating white light by partially absorbing an LED's nearly monochromatic radiation and converting it into a longer wavelength emission through the electronic transitions of the activator ion [3]. The more coverage of the visible spectrum the phosphor/LED combination can achieve, the better the light's color rendering ability and reproduction of an object's true colors [4]. Thus, broadband emitters like Eu^{2+} are among the widely explored activator ions for near complete spectral coverage due to the parity-allowed $4f^7 \leftrightarrow 4f^6 5d^1$ electronic transitions [5]. When Eu^{2+} substitutes for one of the host's crystallographically independent cation sites, the anions (ligands) stabilize the activator's unshielded 5*d* energy levels with two effects. The centroid shift, which is associated with the polarizability of the ligands, decreases the energy of the 5*d* levels of the lanthanide ion by increasing the covalency between the activator and the ligands [6]. The lowest excited $5d_1$ level emerges from a second concurrent effect where crystal field splitting separates the degenerate 5*d* levels, depending on the activator ion-ligand bond length and geometry [7]. Based on these phenomena, oxides such as silicates, aluminates, and borates have been widely studied as hosts for solid-state lighting since they generate a strong enough centroid shift and crystal field splitting to decrease the energy gap between the 4*f* ground and 5*d* lowest excited states emitting in the visible part of the electromagnetic spectrum. They are also all chemically robust with respect to decomposition and easy and cheap to make [8–10].

Phosphates have also captured significant attention not only for their low costs, insolubility in water, and low toxicity but also due to their diverse crystal chemistry, attributed to the adaptability of the tetrahedral $[PO_4]^{3-}$ unit [11]. Connecting four oxygen atoms to different cations or other $[PO_4]^{3-}$ tetrahedral units lead to an array of structures, including chains [12], rings [13], and networks [14]. As a result of the structural diversity, phosphate-based phosphors have yielded

* Corresponding author. Department of Chemistry, University of Houston, Houston, TX, 77204, USA.
E-mail address: jbrgoch@central.uh.edu (J. Brgoch).

https://doi.org/10.1016/j.omx.2023.100257
Received 29 June 2023; Received in revised form 20 July 2023; Accepted 29 July 2023
Available online 11 August 2023
2590-1478/© 2023 The Authors. Published by Elsevier B.V. This is an open access article under the CC BY-NC-ND license (http://creativecommons.org/licenses/by-nc-nd/4.0/).

interesting optical properties. For example, $Na_3Sc_2(PO_4)_3:Eu^{2+}$ shows zero thermal quenching in the temperature range between 25 °C and 200 °C due to the reversible phase transition [15]. Also, its blue emission (λ_{em} = 453 nm) does not shift with increasing temperature while maintaining a photoluminescent quantum yield (PLQY) of around 74%. $K_2BaCa(PO_4)_2:Eu^{2+}$ is also thermally stable, showing zero quenching from 25 °C to 300 °C due to defect de-trapping [16]. Recently, the Whitlockite family phosphates of the formula $A_9RE(PO_4)_7$ and $A_8BRE(PO_4)_7$ (A = Ca, Sr; B=Mg, Zn; RE = Y, Gd, Sc, Lu, In, La) with five cation crystallographically independent sites have been reported as phosphors that can generate an ultra-broad red, yellow, and blue emission band under 365 nm and 400 nm excitation [17–25]. Most notably, a yellow-emitting $Sr_8MgY(PO_4)_7:Eu^{2+}$ was reported with near-UV to violet excitation and a 200 nm (5800 cm^{-1}) full-width-at-half-maximum (*fwhm*) [20]. The broadness of this emission enables a high color rendering index(CRI) daylight bulb fabrication without an additional red-emitting phosphor. The compositional diversity of Whitlockite phosphates can also yield exciting properties by varying the elemental contents by creating solid solutions. Indeed, solid solutions are one of the strategies to control photoluminescent properties by modifying the environment of the cation site [26]. For example, the reported Whitlockite solid solutions of $xSr_2Ca(PO_4)_2-(1-x)Ca_{10}Li(PO_4)_7:Eu^{2+}$ reveals emission color change from blue to greenish-yellow due to the changes on $[Li(4)O_6]$ sites with the introduction of Sr^{2+} causing half of the Li^+ sites to become vacancies and the other half to distort structurally [27].

Although many types of Whitlockite have been studied so far, there appear to be no examples of Ba^{2+}-containing products. The emission colors of these phosphates are also primarily distributed among all colors except for green [28]. These two scientific gaps can be addressed simultaneously by taking a yellow-emitting phosphor and reducing crystal field splitting by substituting a large cation like Ba^{2+} into the host crystal structure. Therefore, in this work, the series of Whitlockite solid solutions were targeted to create a green-emitting phosphor by expanding the unit cell of the reported yellow-emitting $Sr_8MgY(PO_4)_7:Eu^{2+}$ phosphor. This $(Sr_{8-x}Ba_x)_{0.99}Eu_{0.08}MgY(PO_4)_7$ (x = 0, 1, 2, 3) series was investigated by a combination of structural and spectroscopic techniques. X-ray diffraction was performed to verify the material purity with scanning electron microscopy (SEM) and X-ray photoelectron spectroscopy (XPS), supporting the compositional analysis. Diffuse reflectance spectroscopy was employed to estimate the bandgaps of the host structure, while photoluminescence spectroscopy revealed a counterintuitive evolution from greenish-yellow to yellow luminescence upon ion substitution. The shift in emission color is understood through the analysis of the optical properties. The Ba^{2+} substitution also shows that chromatic stability improves with decreasing chromaticity drift at elevated temperatures. The emission spectrum of a prototype pc-LED device with $(Sr_7Ba)_{0.99}Eu_{0.08}MgY(PO_4)_7$, the highest PLQY phosphor among the series, was finally measured, demonstrating nearly complete coverage of the visible spectrum when paired with a violet LED and a cyan- and red-emitting phosphor.

2. Experimental procedure

2.1. Synthesis

The Whitlockite solid solution was prepared following $(Sr_{8-x}Ba_x)_{0.99}Eu_{0.08}MgY(PO_4)_7$ (x = 0, 1, 2, 3) using high-temperature solid-state reactions starting from $SrCO_3$ (Alfa Aesar, 99.99%), $BaCO_3$ (Johnson Mathey, 99.99%), MgO (Sigma-Aldrich, 99.995%), Y_2O_3 (Alfa Aesar, 99.9%), $NH_4H_2PO_4$ (Acros Organics, 99.9%), and Eu_2O_3 (Alfa Aesar, 99.99%). Each component was weighed out in the appropriate stoichiometric ratio with an additional 5 wt % of H_3BO_3 added as a mineralizer (flux). The starting reagents were ground in agate mortar and pestle using acetone as a wetting medium. Powders were further milled for 30 min in a high-energy ball mill (Spex 800 M Mixer/Mill). The mixtures were pressed into a 6 mm diameter pellet and placed on a bed of sacrificial powder in an alumina crucible. The pellets were heated to 1300 °C for 8 h with a heating and cooling rate of 3 °C/min under flowing 5% H_2/95% N_2 gas. After the first heating, the pellets were re-ground and pelletized again. The pellets were heated a second time to 1300 °C for 8 h under the same conditions as the first heating step yielding the final product.

$Na_{1.96}Eu_{0.02}MgPO_4F$ was prepared following published synthetic conditions [31]. Na_2CO_3 (Sigma-Aldrich, 99.95%), MgO (Sigma-Aldrich, 99.995%), $NH_4H_2PO_4$ (Acros Organics, 99.9%), MgF_2 (Sigma-Aldrich, 99.99%) and Eu_2O_3 (Alfa Aesar, 99.99%) were weighed out in the appropriate stoichiometric ratio with an additional 7.5 wt% of Na_2CO_3 to compensate for evaporation during reaction. The starting materials were ground in an acetone medium with an agate mortar and pestle and milled with a high-energy ball mill. The powder was pelletized in a 6 mm diameter and placed in an alumina crucible with sacrificial powder. The pellet was heated at 825 °C for 8 h with a heating and cooling rate of 3 °C/min under flowing 5% H_2/95% N_2 gas.

2.2. Characterization

Powder X-ray diffractograms of both products were collected using an X'Pert PANalytical Empyrean 3 equipped with Cu Kα (λ = 1.5406 Å) as the radiation source. Le Bail refinements were performed using the General Structural Analysis System (GSAS) software and the EXPGUI interface [29]. The background was described using a shifted-Chebyshev function with the peak shapes modeled by a pseudo-Voigt function. Scanning electron microscopy (SEM) micrographs and energy-dispersive X-ray spectroscopy (EDS) elemental mappings were collected using a Phenom Pharos scanning electron microscope attached with a 25 mm^2 silicon drift detector energy-dispersive X-ray spectrometer (Thermo Fisher Scientific). An accelerating voltage of 15 keV and an emission current of 12 μA were used. The Eu concentration was determined by XPS using a Physical Electronics PHI 5700 ESCA System.

Photoluminescence measurements involved mixing the polycrystalline products in an optically transparent silicon epoxy (United Adhesives Inc., OP 4036) and depositing the combination onto a quartz slide (Chemglass). Photoluminescent excitation and emission and temperature-dependent luminescence measurements were obtained using a PTI fluorescence spectrophotometer with a 75 W xenon arc lamp for excitation. A Janis cryostat (VPF-100) was employed to establish a temperature-controlled environment from 80 K to 600 K. The PLQY was determined following the method of de Mello et al. [30], using a Spectralon-coated integrating sphere (150 mm diameter, Labsphere) with an excitation wavelength of 400 nm. Photoluminescent lifetimes were measured using NanoLED N-360 nm LED equipped with the Horiba DeltaFlex Lifetime system (λ_{ex} = 360 nm). Diffuse reflectance spectra were collected using Agilent Technologies Cary 5000 UV–Vis–NIR Spectrophotometer.

The construction of a prototype pc-wLED involved using $(Sr_7Ba)_{0.99}Eu_{0.08}MgY(PO_4)_7$ as the yellow-green component, commercially available $CaAlSiN_3:Eu^{2+}$ as the red phosphor, and $Na_{1.96}Eu_{0.02}MgPO_4F$ as the cyan phosphor. The three phosphors were weighed out with a ratio of 15:1:10, respectively, ground in an agate mortar, and mixed in silicone resin. The resin was formed into a phosphor cap in a custom brass mold and excited using a 400 nm LED driven by a forward bias of 20 mA. The white light spectrum of the prototype was collected and characterized using an Avasphere-5-IRRAD spectrophotometer and AvaSoft 8 software.

3. Results and discussion

3.1. Structural characterization of $(Sr_{8-x}Ba_x)_{0.99}Eu_{0.08}MgY(PO_4)_7$

The original report of the pure host structure, $Sr_8MgY(PO_4)_7$, was previously synthesized at 1300 °C for 8 h [20]. These same conditions here yielded a phase pure, highly crystalline product. However, this

synthetic condition led to unidentified impurities following the substitution of Ba^{2+}. The $Sr_{8-x}Ba_xMgY(PO_4)_7$ series required the inclusion of H_3BO_3 as a mineralizer to obtain pure phase products, as confirmed by powder X-ray diffraction. The mineralizer also improved sample crystallinity. The reported crystal structure of $Sr_8MgY(PO_4)_7$ is isostructural, with $Sr_9In(PO_4)_7$ adopting the proposed monoclinic space group *I2/a*. The structure should contain five crystallographically different Sr^{2+}/Ba^{2+} sites; [Sr/Br(1)O_9], [Sr/Br(2)O_9], [Sr/Br(3)O_9], [Sr/Br(4)O_8], [Sr/Br(5)O_9], and one Y^{3+} site, [Y(1)O_6] [32]. Le Bail refinements of the $Sr_{8-x}Ba_xMgY(PO_4)_7$ series were performed with $Sr_9In(PO_4)_7$ structure file (ICSD #59722) as the starting point. All peaks in the $Sr_{8-x}Ba_xMgY(PO_4)_7$ (x = 0, 1, 2, 3) diffractograms agree with the reference pattern. Incremental Ba^{2+} incorporation shifts the peak positions to smaller 2θ, supporting that the larger Ba^{2+} replaces the smaller Sr^{2+} in the crystal structure (Ba^{2+}: $r_{8\text{-coord}}$ = 1.42 Å, $r_{9\text{-coord}}$ = 1.47 Å; Sr^{2+}: $r_{8\text{-coord}}$ = 1.26 Å, $r_{9\text{-coord}}$ = 1.31 Å) [33]. As shown in Fig. 1b, the unit cell volume of $Sr_{8-x}Ba_xMgY(PO_4)_7$ linearly increases with increasing x through an anisotropic expansion of the structure, where b and β increase by 9% and 7%, respectively, and a and c decrease by 8% and 14%. Ba^{2+} thus distorts the unit cell (Table S1). By x = 4, the diffractogram shows a completely different pattern with fewer peaks implying a higher-symmetry product was obtained and the limit of Ba^{2+} in this phosphate (Fig. S1).

The bandgap of the host structure plays a vital role in the possible photoluminescent excitation and emission properties. The $4f \leftrightarrow 5d$ electronic transitions of Eu^{2+} phosphors are generally between ~2 eV and ~3.5 eV [34]. Host structures thus must have a bandgap at least larger than ~3.5 eV to observe Eu^{2+} luminescence and minimalize the probability of non-radiative transitions, such as thermally-activated photoionization. Considering the difference in ionicity between Sr^{2+} and Ba^{2+}, the bandgaps of a material may change across a solid solution. Diffuse reflectance spectra were collected to determine the bandgap of the unsubstituted $Sr_{8-x}Ba_xMgY(PO_4)_7$ hosts (Fig. S2). All host materials show absorption in the 300 nm region. The bandgap was then estimated by transforming the data into absorption using the Kubelka-Munk function and analyzed by the Tauc relation. The Kubelka-Munk function (**Equation (1)**) approximates diffuse reflectance in the case of semi-infinite samples,

$$F(R_\infty) \equiv \frac{K}{S} = \frac{(1-R_\infty)^2}{2R_\infty} \quad (1)$$

where R_∞ is the diffuse reflectance, K is the absorption coefficient, and S is the scattering coefficient [35]. Under the assumption that incident radiation perfectly diffuses, K becomes equal to 2 α, which is a linear absorption coefficient, and S is a constant with respect to wavelength. Then, the Tauc relation is given by **Equation (2)**,

$$[F(R_\infty)h\nu]^\alpha = A(h\nu - E_g) \quad (2)$$

where ν is light frequency, and A is the proportionality constant. The α is 2 for direct bandgap materials and 1/2 for indirect bandgap materials. The $Sr_{8-x}Ba_xMgY(PO_4)_7$ data were best fit using an $\alpha = 1/2$. As shown in Fig. 2c–f, the resulting band gaps show a slight decrease in the bandgap following Ba^{2+} substitution. This observation is surprising, considering Ba^{2+} should lead to longer, more ionic interactions in the crystal structure. Nevertheless, all the bandgaps remain wide enough to avoid putting the activator's excited energy level in the host structure's conduction band, thereby preventing complete photoluminescence quenching [36].

The $(Sr_{8-x}Ba_x)_{0.99}Eu_{0.08}Mg\ Y(PO_4)_7$ (x = 0, 1, 2, 3) series of phosphors were subsequently prepared following the same synthetic method as used for the phase pure hosts. The phosphor diffractograms match the respective host structure data supporting their phase purity (Fig. S3). Based on the similar ionic radius of Eu^{2+} ($r_{8\text{-coord}}$ = 1.25 Å, $r_{9\text{-coord}}$ = 1.3 Å), isovalency, coordination number, and observed peak shift, Eu^{2+} is considered to replace Sr^{2+}/Ba^{2+} sites, as expected. X-ray diffraction of the phosphors demonstrates a near-phase purity but does not provide information on possible elemental contamination or the final composition. Thus, XPS was performed on the nominally loaded $Sr_{7.92}Eu_{0.08}MgY(PO_4)_7$ sample. The survey spectrum shows that only loaded starting elements are present in the product, indicating no contamination from the synthesis (Fig. 2a). In particular, there was no residual boron from the boric acid mineralizer or aluminum from the crucible. The high-resolution (HRES) spectrum was also collected to estimate the concentration of Eu^{2+} in $Sr_{7.92}Eu_{0.08}MgY(PO_4)_7$. The resulting measured composition was $Sr_{8.7}Eu_{0.09}Mg_{1.7}Y_{0.9}P_{6.6}O_{27.3}$, in agreement with expectation. The four peaks of Eu 3*d* are from $3d_{3/2}$ and $3d_{5/2}$ of Eu^{3+}

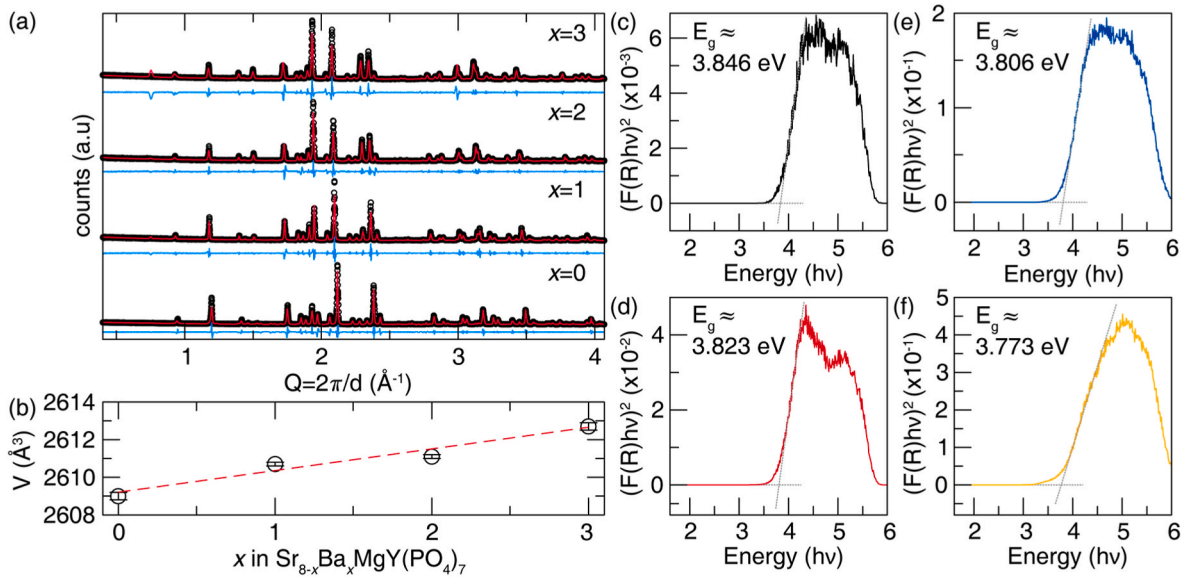

Fig. 1. (a) Le Bail refinements of unsubstituted $Sr_{8-x}Ba_xMgY(PO_4)_7$ (x = 0, 1, 2, 3) starting from the parent $Sr_9In(PO_4)_7$ (ICSD #59722) structure. Black circles represent the measured data, red lines are the fit, and blue lines represent the difference. (b) Calculated volume of $Sr_{8-x}Ba_xMgY(PO_4)_7$ gradually increases with increment Ba^{2+}. Tauc plot of $Sr_{8-x}Ba_xMgY(PO_4)_7$ hosts for (c) x = 0, (d) x = 1, (e) x = 2, and (f) x = 3 used to estimate the bandgap by diffuse reflectance spectroscopy. (For interpretation of the references to color in this figure legend, the reader is referred to the Web version of this article.)

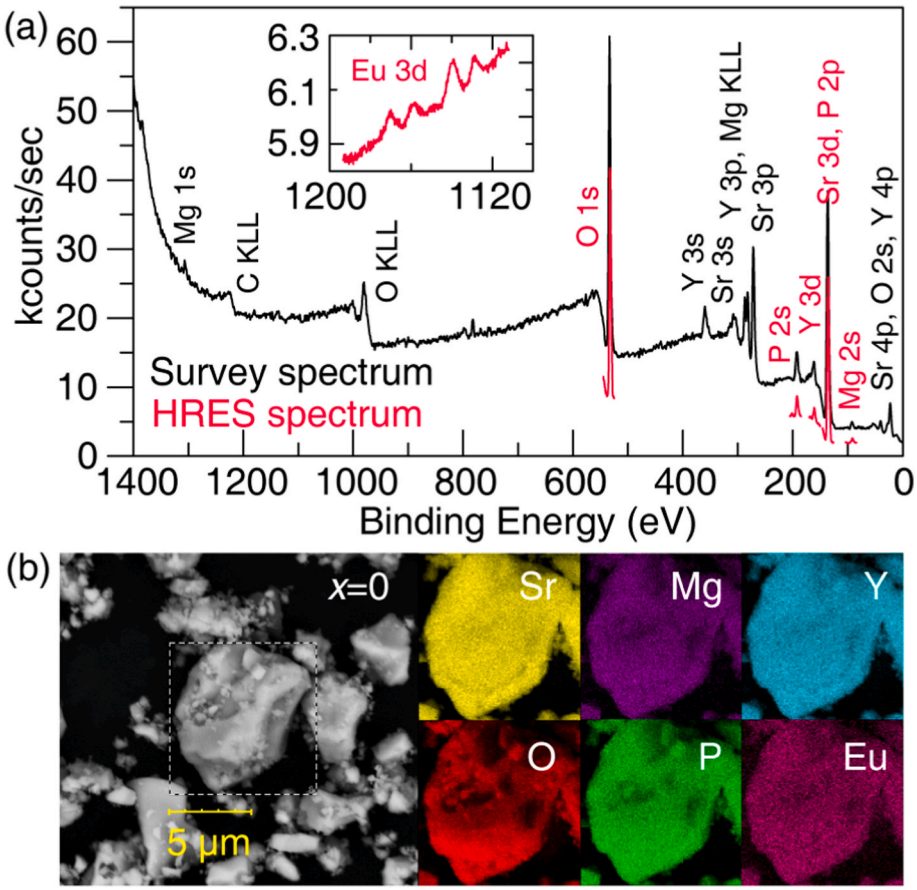

Fig. 2. (a) XPS spectra and (b) EDS micrograph for elemental analysis of $Sr_{7.92}Eu_{0.08}MgY(PO_4)_7$ to provide elemental purity and distribution.

and Eu^{2+}. However, the absence of Eu^{3+} photoluminescence under λ_{ex} = 394 nm suggests that the Eu^{3+} signals from XPS were primarily produced on the surface rather than in the bulk material (Fig. S4). EDS micrographs additionally show that all elements are uniformly distributed in the examined particles indicating no bulk phase/elemental separation (Fig. 2b).

3.2. *Spectroscopic properties of* $(Sr_{8-x}Ba_x)_{0.99}Eu_{0.08}MgY(PO_4)_7$

Substituting Eu^{2+} into the $Sr_{8-x}Ba_xMgY(PO_4)_7$ (x = 0, 1, 2, 3) solid solution leads to yellow luminescence within the excitation band spanning from 280 nm to 440 nm. Diffuse reflectance of the $(Sr_{8-x}Ba_x)_{0.99}Eu_{0.08}MgY(PO_4)_7$ phosphors show that substituting Eu^{2+} generates absorption from 350 nm to 400 nm, corresponding to the $4f^7 \rightarrow 4f^6 5d^1$ transition (Fig. S2). The photoluminescent emission spectra of $(Sr_{8-x}Ba_x)_{0.99}Eu_{0.08}MgY(PO_4)_7$ (x = 0, 1, 2, 3) are presented in Fig. 3a. A comparison of normalized spectra shows more clearly that increasing the Ba^{2+} content caused the emission peak center to shift towards longer wavelengths from 512 nm to 533 nm (Fig. S5). Calculating the *fwhm* indicates a slight decrease with increasing Ba^{2+} content from 188 nm (5905 cm^{-1}) at x = 0–175 nm (5428 cm^{-1}) at x = 3. This small change is still sufficiently broad to cover a large portion of the visible spectrum.

The emission spectrum can be deconvoluted into two Gaussian functions, with the peaks centered at 509 nm (19,646 cm^{-1}) and 598 nm (16,722 cm^{-1}). Intriguingly, Huang et al. [20] originally decomposed the emission spectrum of $Sr_8MgY(PO_4)_7:Eu^{2+}$ into five Gaussian peaks. Here, describing the data by more than two Gaussians resulted in overfitted and overlapping peaks. The analysis suggests that the five crystallographically independent sites can be better classified into two groups based on the respective coordination numbers: all 9-coordinated sites have spectroscopically indistinguishable polyhedral environments for Eu^{2+}. These 9-coordinated sites correspond to a shorter wavelength peak due to weaker crystal field splitting than the 8-coordinated site, producing the observed longer wavelength emission [37]. Increasing the Ba^{2+} content causes the first peak to gradually shift to longer wavelengths (x = 1, $\lambda_{em,max}$ = 513 nm; x = 2, $\lambda_{em,max}$ = 515 nm; x = 3, $\lambda_{em,max}$ = 516 nm), whereas the second 8-coordinated peak remains centered around 600 nm (Table S2). The CIE chromaticity coordinates of each emission spectra indicate a slight shift from greenish-yellow (0.333, 0.441) to yellow (0.351, 0.464) (Fig. 3b). The emission spectra also change under different excitation wavelengths, with the first emission peak excited by shorter wavelengths. In contrast, lower energy excitation is associated with the second lower energy peak emission peak, further supporting the substitution site assignments based on crystal field splitting arguments (Fig. S6).

Further insight into the spectroscopic properties of investigated materials was obtained from luminescent lifetime measurements. As presented in Fig. S7, all decays can be described with a bi-exponential function having lifetimes of τ_1 = 300 ns and τ_2 = 1.6 μs, further corroborating the decomposition with two Gaussian functions of emission spectra. Although τ_1 seems short for Eu^{2+} substituted phosphors, other phosphates have also been reported with short lifetimes of a few hundred nanoseconds [38]. This short lifetime benefits pc-wLEDs by reducing the saturation effects, but further work is needed to understand why there is such a significant difference between the lifetimes of the two emission peaks [39,40].

This material shows a desirable broad yellow emission. However, it must also have good photon conversion efficiency to be applied in actual devices. The photoluminescence quantum yield of $(Sr_{8-x}Ba_x)_{0.99}Eu_{0.08}MgY(PO_4)_7$ (x = 0, 1, 2, 3) phosphors was evaluated by measuring the PLQY at different Ba^{2+} concentrations. As plotted in Fig. 3c, the sample containing x = 1 shows the highest PLQY of 48(1)%,

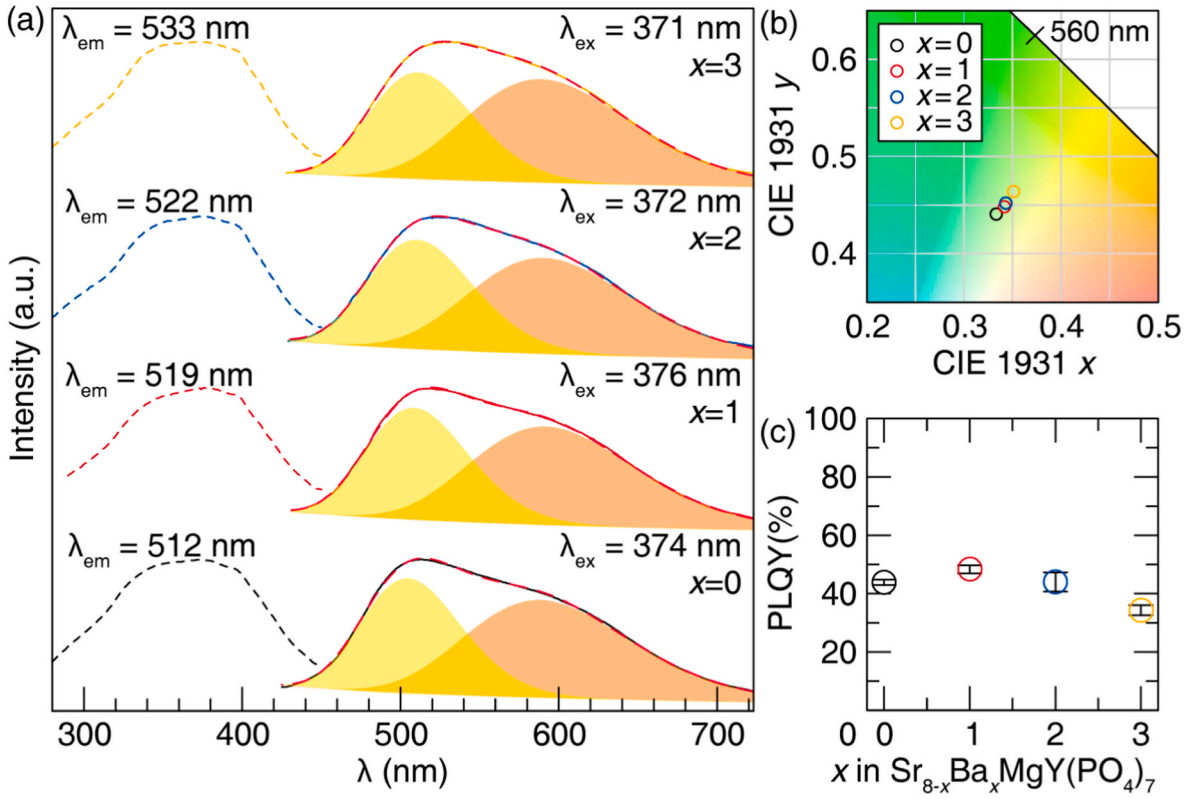

Fig. 3. (a) Excitation and mission spectra recorded at room temperature, (b) emission color change in CIE 1931 space, and (c) Room temperature PLQY of $(Sr_{8-x}Ba_x)_{0.99}Eu_{0.08}MgY(PO_4)_7$ ($x = 0, 1, 2, 3$).

a moderate value for unoptimized products. Further increasing the Ba^{2+} concentration leads to decreasing PLQY value to 34(2)% for $(Sr_5Ba_3)_{0.99}Eu_{0.08}MgY(PO_4)_7$.

Considering current LED chips operate at elevated temperatures (≈423 K), a phosphor must maintain the same luminescence as temperature increases [41]. Therefore, the thermal and chromatic stability of the $(Sr_{8-x}Ba_x)_{0.99}Eu_{0.08}MgY(PO_4)_7$ ($x = 0, 1, 2, 3$) phosphors were measured from 80 K to 600 K (Fig. S8). As the temperature increases, the emission intensity in the investigated materials starts to decrease due to thermal quenching above about 300 K. The thermal quenching temperature, or the temperature at which the intensity of luminescence equals 50% of its original value at low temperature (T_{50}), was estimated by plotting the normalized integrated area of each emission spectrum. As shown in Fig. 4a, all compositions have estimated T_{50} values hovering between 400 K–420 K. Although this is not ideal, falling right at the DOE lower limit of 423 K, it is still reasonable to consider the material for proof-of-concept device construction. Analyzing the emission peaks also shows chromatic stability with minimal shifts in the emission peak

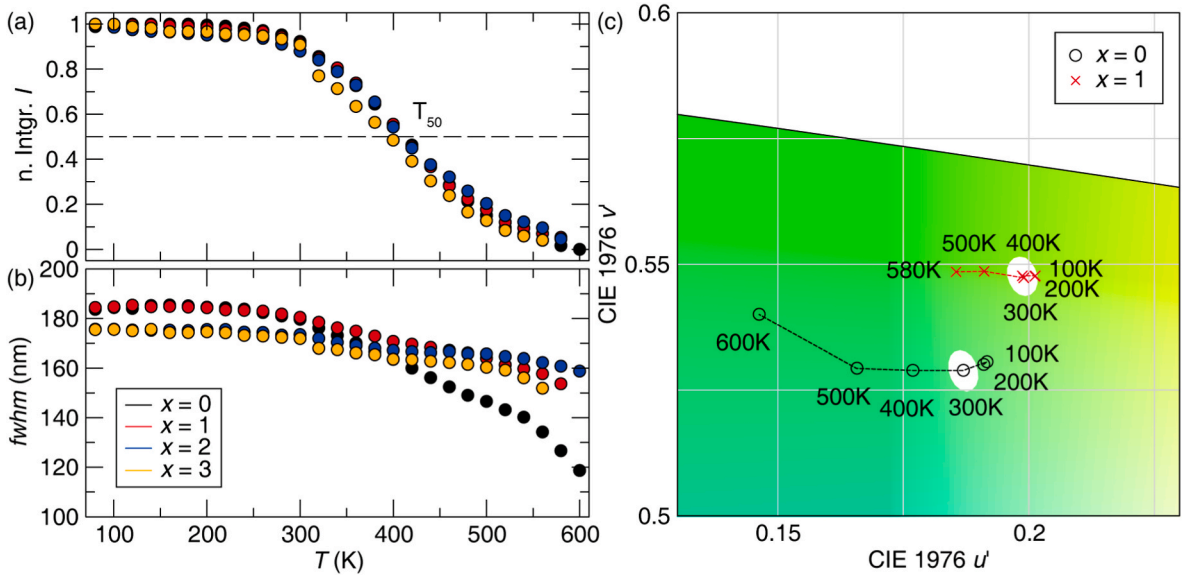

Fig. 4. Comparing changes in (a) normalized integrated intensity and (b) *fwhm* of $(Sr_{8-x}Ba_x)_{0.99}Eu_{0.08}MgY(PO_4)_7$ ($x = 0, 1, 2, 3$) along temperature; (d) Changes in chromaticity by increasing temperature in CIE 1976 space of $(Sr_{8-x}Ba_x)_{0.99}Eu_{0.08}MgY(PO_4)_7$ ($x = 0, 1$).

maximum as a function of temperature. The presence of Ba^{2+} appears to cause only minor changes in the *fwhm,* with the peak narrowing slightly up to 600 K (Fig. 4b). This is vital because even subtle shifts in the emission maximum or *fwhm* can lead to notable shifts in the perceived color of the phosphor. In Fig. 4c, the color shifts are plotted as a function of increasing temperature for $Sr_{7.92}Eu_{0.08}MgY(PO_4)_7$ and $(Sr_7Ba)_{0.99}Eu_{0.08}MgY(PO_4)_7$. A 3-step MacAdam ellipse is presented as a white oval centered at each phosphor's 300 K color coordinates (Fig. 4c). The shift in emission color of $(Sr_7Ba)_{0.99}Eu_{0.08}MgY(PO_4)_7$ ($x = 1$) is barely distinguishable in the temperature range from 100 K to 400 K since the corresponding data points fall within the MacAdam ellipse, supporting the chromatic stability. However, once the temperature increases above 400 K, there is a more notable change in the emission color. This is in contrast to $Sr_{7.92}Eu_{0.08}MgY(PO_4)_7$ ($x = 0$), which shows a significant shift moving away from 300 K. This origin of this change is evident by looking at the change in the *fwhm* (Fig. 4b). The emission peak narrows significantly at higher temperatures even though the emission peak position is reasonably stable, leading to the observed change in emission color. Thus, the presence of Ba^{2+} is beneficial for the chromatic stability of this phosphor.

The activation energy responsible for quenching can be calculated using the Arrhenius equation, as depicted by **Equation (3)**,

$$I(T) = \frac{I_0}{1 + Ae^{\left(-\frac{E_a}{kT}\right)}} \tag{3}$$

where I_0 is the initial intensity, E_a is the activation energy, k is the Boltzmann constant, and T is the temperature. Fig. S9 presents the calculated activation energies for $(Sr_{8-x}Ba_x)_{0.99}Eu_{0.08}MgY(PO_4)_7$ ($x = 0,1,2,3$) series of solid solutions. At $x = 1$, E_a has the highest value of 0.292 eV. With a higher Ba^{2+} component, it decreases to 0.268 eV ($x = 3$), showing a similar tendency with T_{50}. Those values can be considered reasonable for thermally stable phosphors since other thermally stable phosphors show similar values between 0.24 eV and 0.29 eV [42,43].

Finally, $(Sr_7Ba)_{0.99}Eu_{0.08}MgY(PO_4)_7$ with the highest quantum yield was further selected for temperature-dependent lifetime measurement. The decay curves are well described with a bi-exponential function and show similar lifetime kinetics until the temperature reaches 280 K (Fig. S10). At higher temperatures, both values of lifetimes decrease by 68% and 86%, respectively, due to the thermally-induced increased probability of non-radiative transitions. Two T_{50} values from lifetime are around 420 K, consistently with T_{50} derived from emission spectra.

3.3. Device fabrication incorporating the $Sr_7BaEu_{0.08}MgY(PO_4)_7$ phosphor

The performance of the $(Sr_7Ba)_{0.99}Eu_{0.08}MgY(PO_4)_7$ phosphor was evaluated by creating a prototype device. This involved constructing a phosphor blend that covered the entire visible spectrum to generate a white pc-LED device. In this case, a violet LED chip ($\lambda_{ex} = 400$ nm) was combined with a mixture of the cyan-emitting $Na_2MgPO_4F:Eu^{2+}$, the green-yellow emitting $(Sr_7Ba)_{0.99}Eu_{0.08}MgY(PO_4)_7$, and red-emitting $CaAlSiN_3:Eu^{2+}$ phosphors. $(Sr_7Ba)_{0.99}Eu_{0.08}MgY(PO_4)_7$ was chosen due to the highest PLQY (≈ 48(1)%) and reasonable color stability. This combination of phosphors was combined in a silicon mold to produce a phosphor cap driven by a 20 mA diode. The resulting photoluminescence spectrum is plotted in Fig. 5a. The spectrum covers almost the whole visible region of the electromagnetic range. Plotting the color point of this device on 1931 CIE coordinates shows the light falls near

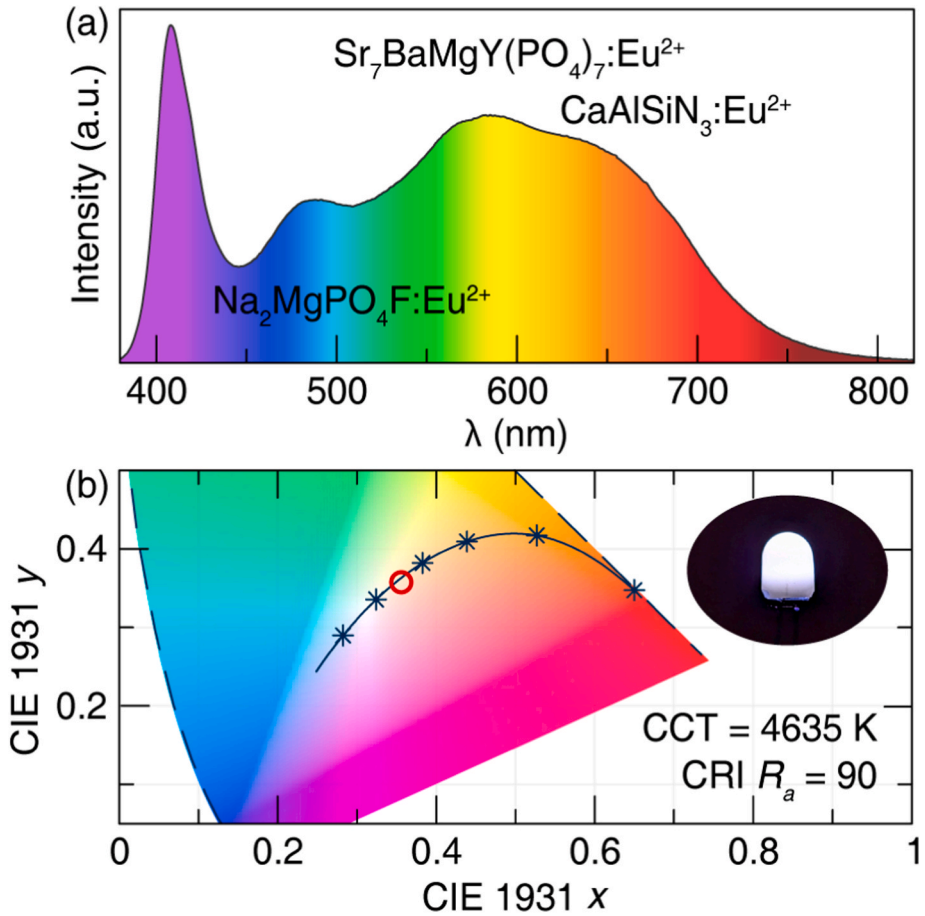

Fig. 5. (a) The emission spectrum of a device constructed of $(Sr_7Ba)_{0.99}Eu_{0.08}MgY(PO_4)_7$, $Na_2MgPO_4F:Eu^{2+}$, $CaAlSiN_3:Eu^{2+}$, and 400 nm LED (b) the CIE coordinates of the device.

the Plankian locus with (x, y)=(0.356, 0.357). This constructed device has a CRI = 90 and a color correlated temperature (CCT) of 4635 K, indicating that daylight white lighting can be generated with good color quality using this phosphor.

4. Conclusion

In summary, the solid solution of yellow-emitted $(Sr_{8-x}Ba_x)_{0.99}Eu_{0.08}MgY(PO_4)_7$ (x = 0, 1, 2, 3) phosphors were successfully synthesized, and their structural and luminescence properties were investigated. The excitation spectra exhibit broadband excitation in the 250 nm–450 nm range in near-UV regions. Under 400 nm excitation, the emission spectrum shifts from greenish-yellow to yellow luminescent with a fair PLQY of ~40%–50%. Two crystallographically independent types of Eu^{2+} with different coordination environments were identified by the deconvolution of emission spectra into two Gaussian functions and supported by biexponential photoluminescence decay measurements. Ba^{2+} incorporation improved thermal stability in $(Sr_7Ba)_{0.99}Eu_{0.08}MgY(PO_4)_7$, with the highest T_{50} of 420 K and chromatic stability between 100K and 400K. The highest E_a value supports the thermal quenching trends. Fabricating an LED device with $(Sr_7Ba)_{0.99}Eu_{0.08}MgY(PO_4)_7$ generated a daylight white color with a CRI value of 90, demonstrating that $(Sr_{8-x}Ba_x)_{0.99}Eu_{0.08}MgY(PO_4)_7$:$Eu^{2+}$ (x = 0, 1, 2, 3) can be a phosphor for white LED.

Notes

The authors declare no competing financial interest.

CRediT authorship contribution statement

Nakyung Lee: Conceptualization, Methodology, Formal analysis, Investigation, Data curation, Writing – original draft, Visualization. **Małgorzata Sójka:** Validation, Formal analysis, Writing – original draft, Writing – review & editing. **Jakoah Brgoch:** Validation, Resources, Writing – review & editing, Supervision, Project administration, Funding acquisition.

Declaration of competing interest

The authors declare the following financial interests/personal relationships which may be considered as potential competing interests:

Jakoah Brgoch reports financial support was provided by National Science Foundation (DMR-1847701).

Data availability

Data will be made available on request.

Acknowledgments

The authors thank Dr. Boris Makarenko for collecting XPS data and the National Science Foundation (DMR-1847701) for supporting this work.

Appendix A. Supplementary data

Supplementary data to this article can be found online at https://doi.org/10.1016/j.omx.2023.100257.

References

[1] H.A. Höppe, Recent developments in the field of inorganic phosphors, Angew. Chem. Int. Ed. 48 (2009) 3572–3582, https://doi.org/10.1002/anie.200804005.
[2] C.C. Lin, R.S. Liu, Advances in phosphors for light-emitting diodes, J. Phys. Chem. Lett. 2 (2011) 1268–1277, https://doi.org/10.1021/jz2002452.
[3] P.F. Smet, A.B. Parmentier, D. Poelman, Selecting conversion phosphors for white light-emitting diodes, J. Electrochem. Soc. 158 (2011) R37, https://doi.org/10.1149/1.3568524.
[4] W. Davis, Y. Ohno, Approaches to color rendering measurement, J. Mod. Opt. 56 (2009) 1412–1419, https://doi.org/10.1080/09500340903023733.
[5] M. Zhao, Q. Zhang, Z. Xia, Structural engineering of Eu^{2+} doped silicates phosphors for LED applications, Acc. Mater. Res. 1 (2020) 137–145, https://doi.org/10.1021/accountsmr.0c00014.
[6] P. Dorenbos, Ce^{3+} 5d centroid shift and vacuum referred 4f-electron binding energies of all lanthanide impurities in 150 different compounds, J. Lumin. 135 (2013) 93–104, https://doi.org/10.1016/j.jlumin.2012.09.034.
[7] P. Dorenbos, Crystal field splitting of lanthanide 4f 5d-levels in inorganic compounds. www.elsevier.com/locate/jallcom, 2002.
[8] S. Adachi, Review—photoluminescence properties of Cr^{3+} activated oxide phosphors, ECS Journal of Solid State Science and Technology 10 (2021), 026001, https://doi.org/10.1149/2162-8777/abdc01.
[9] S. Adachi, Photoluminescence properties of Mn^{4+} activated oxide phosphors for use in white-LED applications: a review, J. Lumin. 202 (2018) 263–281, https://doi.org/10.1016/j.jlumin.2018.05.053.
[10] R.C. Ropp, Spectral properties of rare earth oxide phosphors, J. Electrochem. Soc. 111 (1964) 311, https://doi.org/10.1149/1.2426114.
[11] K.N. Shinde, S.J. Dhoble, H.C. Swart, K. Park, Basic Mechanisms of Photoluminescence, 2012, pp. 41–59, https://doi.org/10.1007/978-3-642-34312-4_2.
[12] L.S. Ivashkevich, A.S. Lyakhov, A.F. Selevich, Crystal structure of gallium and chromium salts belonging to the family $M^{III}H_2P_3O_{10}{\cdot}2H_2O$, Phosphorus Research Bulletin 24 (2010) 6–11, https://doi.org/10.3363/prb.24.6.
[13] N.N. Chudinova, L.A. Borodina, E. V Murashova, Neodymium cyclohexaphosphates in the $NdCl_3$-$Li_6P_6O_{18}$-H_2O system, Inorg. Mater. 38 (2002) 1520–1524, https://doi.org/10.1023/A:1021387808037.
[14] A. Olbertz, D. Stachel, I. Svoboda, H. Fuess, $NiHP_5O_{14}$ ultraphosphate, Acta Crystallogr. C52 (1996) 1603–1605, https://doi.org/10.1107/S0108270196000595.
[15] Y.H. Kim, P. Arunkumar, B.Y. Kim, S. Unithrattil, E. Kim, S.H. Moon, J.Y. Hyun, K. H. Kim, D. Lee, J.S. Lee, W. Bin Im, A zero-thermal-quenching phosphor, Nat. Mater. 16 (2017) 543–550, https://doi.org/10.1038/nmat4843.
[16] J. Qiao, L. Ning, M.S. Molokeev, Y.C. Chuang, Q. Liu, Z. Xia, Eu^{2+} site preferences in the mixed cation $K_2BaCa(PO_4)_2$ and thermally stable luminescence, J. Am. Chem. Soc. 140 (2018) 9730–9736, https://doi.org/10.1021/jacs.8b06021.
[17] C.H. Huang, W.R. Liu, T.M. Chen, Single-phased white-light phosphors $Ca_9Gd(PO_4)_7$:Eu^{2+}, Mn^{2+} under near-ultraviolet excitation, J. Phys. Chem. C 114 (2010) 18698–18701, https://doi.org/10.1021/jp106693z.
[18] D. Kim, Y.W. Seo, S.H. Park, B.C. Choi, J.H. Kim, J.H. Jeong, Theoretical design and characterization of high efficient $Sr_9Ln(PO_4)_7$:Eu^{2+} phosphors, Mater. Res. Bull. 127 (2020), 110856, https://doi.org/10.1016/j.materresbull.2020.110856.
[19] X. Dong, J. Zhang, L. Zhang, X. Zhang, Z. Hao, Y. Luo, Yellow-emitting $Sr_9Sc(PO_4)_7$:Eu^{2+}, Mn^{2+} phosphor with energy transfer for potential application in white light-emitting diodes, Eur. J. Inorg. Chem. (2014) 870–874, https://doi.org/10.1002/ejic.201301216.
[20] C.H. Huang, Y.C. Chiu, Y.T. Yeh, T.M. Chen, Novel Eu^{2+} activated yellow-emitting $Sr_8MgLu(PO_4)_7$ phosphors for white-light near-ultraviolet LEDs, Materials Express 2 (2012) 303–310, https://doi.org/10.1166/mex.2012.1081.
[21] C.H. Huang, D.Y. Wang, Y.C. Chiu, Y.T. Yeh, T.M. Chen, $Sr_8MgGd(PO_4)_7$:Eu^{2+}: Yellow-emitting phosphor for application in near-ultraviolet-emitting diode based white-light LEDs, RSC Adv. 2 (2012) 9130–9134, https://doi.org/10.1039/c2ra20646c.
[22] Y. Zhong, S. Gai, Y. Yang, M. Xia, Y. Zhang, F. Qiu, F. Xiang, Z. Zhou, A novel green phosphor $Sr_8ZnY(PO_4)_7$:Eu^{2+}, Ln^{3+} (Ln = Pr, Tm, Yb) with broad emission band for high color rendering white-lighting-emitting diodes, J. Lumin. 214 (2019), 116600, https://doi.org/10.1016/j.jlumin.2019.116600.
[23] J. Zhou, M. Chen, J. Zhang, C. Shi, J. Ding, Y. Zhuang, Q. Wu, Regulating photoluminescence behavior by neighboring-cation-size in $Sr_8CaX(PO_4)_7$:Eu^{2+} (X = Al and Ga) phosphors for high color rendering solid-state lighting source, Chem. Eng. J. 426 (2021), 131869, https://doi.org/10.1016/j.cej.2021.131869.
[24] F. Xie, J. Li, Z. Dong, D. Wen, J. Shi, J. Yan, M. Wu, Energy transfer and luminescent properties of $Ca_8MgLu(PO_4)_7$:Tb^{3+}/Eu^{3+} as a green-to-red color tunable phosphor under NUV excitation, RSC Adv. 5 (2015) 59830–59836, https://doi.org/10.1039/c5ra08680a.
[25] C. Zhong, L. Zhang, Y. Xu, X. Wu, S. Yin, X. Zhang, H. You, Design of novel cyan phosphor $Ca_7NaLu(PO_4)_6$:Eu^{2+} for full-visible-spectrum white LED: enhanced thermal stability and tuned emission by neighbor cation effect, Mater. Today Chem. 26 (2022), 101233, https://doi.org/10.1016/j.mtchem.2022.101233.
[26] M. Zhao, Q. Zhang, Z. Xia, Structural engineering of Eu^{2+} doped silicates phosphors for LED applications, Acc. Mater. Res. 1 (2020) 137–145, https://doi.org/10.1021/accountsmr.0c00014.
[27] M. Chen, Z. Xia, M.S. Molokeev, T. Wang, Q. Liu, Tuning of photoluminescence and local structures of substituted cations in xSr2Ca(PO4)2-(1–x)Ca10Li(PO4)7:Eu2+ phosphors, Chem. Mater. 29 (2017) 1430–1438, https://doi.org/10.1021/acs.chemmater.7b00006.
[28] J. Qiao, J. Zhao, Z. Xia, A review on the Eu2+ doped β-Ca3(PO4)2-type phosphors and the sites occupancy for photoluminescence tuning, Opt. Mater. X 1 (2019), https://doi.org/10.1016/j.omx.2019.100019.
[29] B.H. Toby, Expgui, EXPGUI, a graphical user interface for GSAS Applied Crystallography EXPGUI, a graphical user interface for GSAS, J. Appl. Crystallogr. 34 (2001) 210–213.

[30] J.C. de Mello, F.H. Wittmann, R.H. Friend, An improved experimental determination of external photoluminescence quantum efficiency, Adv. Mater. 9 (1994) 230–232, https://doi.org/10.1002/adma.19970090308.
[31] S. Hariyani, J. Brgoch, Advancing human-centric LED lighting using Na_2MgPO_4F:Eu^{2+}, ACS Appl. Mater. Interfaces 13 (2021) 16669–16676, https://doi.org/10.1021/acsami.1c00909.
[32] A.A. Belik, F. Izumi, T. Ikeda, M. Okui, A.P. Malakho, V.A. Morozov, B.I. Lazoryak, Whitlockite-related phosphates $Sr_9A(PO_4)_7$ (A=Sc, Cr, Fe, Ga, and In): structure refinement of $Sr_9In(PO_4)_7$ with synchrotron X-ray powder diffraction data, J. Solid State Chem. 168 (2002) 237–244, https://doi.org/10.1006/jssc.2002.9716.
[33] R.D. Shannon, C.T. Prewitt, Effective ionic radii in oxides and fluorides, Acta Crystallogr. 32 (1963) 751–767, https://doi.org/10.1107/S0567740869003220.
[34] P. Dorenbos, A review on how lanthanide impurity levels change with chemistry and structure of inorganic compounds, ECS Journal of Solid State Science and Technology 2 (2013), https://doi.org/10.1149/2.001302jss. R3001–R3011.
[35] M.L. Myrick, M.N. Simcock, M. Baranowski, H. Brooke, S.L. Morgan, J. N. McCutcheon, The kubelka-munk diffuse reflectance formula revisited, Appl. Spectrosc. Rev. 46 (2011) 140–165, https://doi.org/10.1080/05704928.2010.537004.
[36] P. Dorenbos, Thermal quenching of Eu^{2+} 5d-4f luminescence in inorganic compounds, J. Phys. Condens. Matter 17 (2005) 8103–8111, https://doi.org/10.1088/0953-8984/17/50/027.
[37] S. Wang, Z. Song, Y. Kong, Z. Xia, Q. Liu, Crystal field splitting of 4fn−15d-levels of Ce^{3+} and Eu^{2+} in nitride compounds, J. Lumin. 194 (2018) 461–466, https://doi.org/10.1016/j.jlumin.2017.10.073.
[38] S.H.M. Poort, A. Meyerink, G. Blasse, Lifetime measurements in Eu^{2+} doped host lattices, J. Phys. Chem. Solid. 58 (1997) 1451–1456, https://doi.org/10.1016/S0022-3697(97)00010-3.
[39] M.A. Van De Haar, M. Tachikirt, A.C. Berends, M.R. Krames, A. Meijerink, F. T. Rabouw, Saturation mechanisms in common LED phosphors, ACS Photonics 8 (2021) 1784–1793, https://doi.org/10.1021/acsphotonics.1c00372.
[40] A. Zych, M. De Lange, C. De Mello Donegá, A. Meijerink, Analysis of the radiative lifetime of Pr 3 d-f emission, J. Appl. Phys. 112 (2012), https://doi.org/10.1063/1.4731735.
[41] Clemens J.M. Lasance, Andras Poppe, Thermal Management for LED Applications, Solid State Lighting Technology and Application Series, Springer, 2014, pp. 53–69, in *(chapter 3) Basics of Thermal Design for LEDs*, http://www.springer.com/series/8864.
[42] W.W. Hu, W.W. Ji, S.A. Khan, L.Y. Hao, X. Xu, L.J. Yin, S. Agathopoulos, J. McKittrick, Preparation of $Sr_{1-x}Ca_xLiAl_3N_4$:Eu^{2+} solid solutions and their photoluminescence properties, J. Am. Ceram. Soc. 99 (2016) 3273–3279, https://doi.org/10.1111/jace.14335.
[43] J. Chen, Y. Liu, L. Mei, H. Liu, M. Fang, Z. Huang, Crystal structure and temperature-dependent luminescence characteristics of $KMg_4(PO_4)_3$:Eu^{2+} phosphor for white light-emitting diodes, Sci. Rep. 5 (2015), https://doi.org/10.1038/srep09673.